

Electrical transport in the ferromagnetic state of silver substituted manganites $\text{La}_{1-x}\text{Ag}_x\text{MnO}_3$ ($x = 0.05$ and 0.1)

Dinesh Varshney,^{a)} Dinesh Choudhary, and Elias Khan

Materials Science Laboratory, School of Physics, Devi Ahilya University, Indore 452001, India

(Received 10 May 2014; accepted 9 November 2014)

The present study focuses on a quantitative analysis of electrical resistivity in monovalent-doped manganites $\text{La}_{1-x}\text{Ag}_x\text{MnO}_3$ ($x = 0.05$ and 0.1). The electrical resistivity data in the ferromagnetic (FM) metallic phase are analyzed by considering a temperature-independent inelastic scattering of the electrons (due to domain and grain boundaries, defects, etc.) and other temperature-dependent elastic scattering mechanisms (electron-electron, electron-phonon, and electron-magnon). The Debye and Einstein temperatures are deduced from the model Hamiltonian containing potential energy contribution from the long-range Coulomb, van der Waals (vdW) interaction, and short-range repulsive interaction up to the second-neighbor ions. The electron-phonon scattering partially describes the reported FM metallic resistivity behavior with temperature for $\text{La}_{1-x}\text{Ag}_x\text{MnO}_3$ ($x = 0.05$ and 0.1). The T^2 and $T^{4.5}$ terms accounting for electron-electron and electron-magnon interactions are essential for the correct description of resistivity. The Mott-Ioffe-Regel criterion for metallic conductivity is valid, and $k_{\text{F}} \sim 1$, $\varepsilon_{\text{F}}\tau \sim 1$.

I. INTRODUCTION

Since the discovery of colossal magnetoresistance (CMR) in perovskite manganese oxides $\text{Re}_{1-x}\text{A}_x\text{MnO}_3$ (where Re is a trivalent rare-earth element such as La, Pr, and Nd and A is a divalent metal element such as Ca, Sr, Ba, or Pb), much theoretical and experimental work has been done to investigate the physical mechanism of the CMR effect because of their interesting physical properties and technological importance.¹ The doped manganites are known to exhibit a number of unusual and interesting electronic properties amongst which the temperature-dependent metal-insulator (MI) transition is probably the most dramatic ones. It is established that the spin structure and electronic properties of $\text{Re}_{1-x}\text{A}_x\text{MnO}_3$ are correlated within the framework of the double-exchange mechanism.^{2,3} The double exchange alone could not explain the CMR effects in $\text{Re}_{1-x}\text{A}_x\text{MnO}_3$ and proposed that a strong electron-phonon coupling, e.g., via Jahn-Teller effects, should be effective.⁴

In the recent past, monovalent alkali metal doped $\text{Re}_{1-x}\text{B}_x\text{MnO}_3$ (B = Na, K, Ag, etc.) has also attracted the researchers.^{5,6} As the valence state alkali metal ions is +1, the substitution of these ions affects the ratio of Mn^{3+} ($t_{2g}^3e_g^1$) and Mn^{4+} ($t_{2g}^3e_g^0$) ions, which finally also influences the double exchange mechanism and can give rise to different interplays amongst charge, spin, and lattice

degrees of freedom. The metal ions such as La and Ag are close in ionic radius ($R_{\text{La}}^{3+} = 1.18 \text{ \AA}$, $R_{\text{Ag}}^{+} = 1.13 \text{ \AA}$), and the $\text{La}_{1-x}\text{Ag}_x\text{MnO}_3$ system is of considerable interest.

Raman spectroscopy provided essential information about the lattice and JT distortion and orbital ordering in the manganites that occurs at variable doping levels.⁷ It is also used to elucidate the spin-phonon and electron-phonon interaction present in the system. The ideal perovskite ABO_3 of cubic structure space group $Pm\bar{3}m$ presents 15 normal modes of vibration. On the other hand, doping at La (A) or at Mn (B) site essentially causes a change in the structure which is due to either the mismatch of the ionic radii of the ions in the unit cell or the J-T effect associated with the Mn^{3+} ions. The result is orthorhombic ($Pnma$) and rhombohedral ($\bar{R}\bar{3}c$) structures with Raman active phonon modes.

For higher doping in manganites, the strong electron-phonon coupling localizes the conduction band electrons as polarons. The polaronic effect is reduced as the temperature is decreased through the Curie temperature T_C , permitting the formation of a metallic state.⁸ For doped manganites, it is pointed out that the electron-phonon interactions are substantial and the existence of insulating states competing with the Double exchange induced ferromagnetic (FM) metal is important. Besides the FM metallic phase, the antiferromagnetic (AF) charge-ordered insulating state is necessary to explain the CMR effect.⁹ The AF superexchange J_{AF} coupling plays a crucial role in the magnitude of the CMR effect. The J_{AF} is needed to stabilize the charge ordered AF state that competes with the FM metal. The origin of the CMR effect relies on a nanometer-scale short-range order above T_C . To obtain CMR effects, clusters of just a few lattice spacing in size appear sufficient.¹⁰

Contributing Editor: Ian M. Reaney

^{a)}Address all correspondence to this author.

e-mail: vdinesh33@rediffmail.com

DOI: 10.1557/jmr.2014.400

The monovalent (Na, K, and Ag) doped manganites illustrate the metallic behavior below temperature T_{MI} . Above this temperature, it behaves like a semiconductor. For $\text{La}_{1-x}\text{Ag}_x\text{MnO}_3$, the MI transition temperature T_{MI} increases with the Ag concentration x ($0 < x \leq 0.5$). The T_{MI} is 272 K for $x = 0.05$ and 299 K for $x = 0.1$, respectively.¹¹ The structural and electronic properties of the perovskite crystal clearly have an important effect on magnetoresistance and in particular on the Curie temperature. It has been observed that the interactions between the charge carriers and vibrations of the crystal lattice (phonons) also play a fundamental role in changing the resistance as the temperature falls toward the Curie temperature.

Earlier, Kumar and Majumdar solved the disordered Holstein-double exchange model to study the effect of disorder at strong electron–phonon coupling and noticed that even weak disorder enormously enhances the resistivity at $T = 0$ K, simultaneously suppressing the density of states at the Fermi level. Furthermore, the presence of weak disorder suppresses the temperature-dependent increase of ρ and leads to a regime with $d\rho/dT < 0$, which is attributed to the disorder induced tendency toward polaron formation.¹² Later on, it is demonstrated that the extrinsic disorder controls the interplay of lattice polaron effects and spin fluctuations and leads to widely varying regimes in transport explicitly for optimally doped manganites.¹³

The polaron behaves like heavy particles and can be mobile with metallic conduction at low temperatures and form a polaronic Fermi liquid.¹⁴ The resistivity data of $\text{La}_{1-x}\text{Ca}_x\text{MnO}_3$ below 100 K are consistently retraced by a polaron mechanism. The behavior of resistivity at low temperature in a FM metallic state of manganites is consistent with small-polaron coherent motion that involves a relaxation due to a low-lying optical phonon mode.¹⁵

At low temperatures, a dominant T^2 contribution in resistivity is generally observed and has been ascribed to electron–electron scattering. In manganites, the resistivity is essentially temperature independent below 20 K and exhibits a strong T^2 dependence above 50 K.¹⁶ Kubo and Ohata suggest two-magnon processes, predicting a leading $T^{4.5}$ dependence of the resistivity in the FM phase of manganites.¹⁷ The resistivity peak and the CMR of hole doped manganites $\text{La}_{0.75}\text{Ca}_{0.25}\text{MnO}_3$ are a result of the current carrier density collapse with strong electron–phonon coupling. The FM transition in manganites is driven by an exchange interaction of polaronic carriers with localized spins.¹⁸ In both hole and electron doped manganites, an additional contribution arising from the electron–electron contribution is a must to analyze the FM metallic resistivity behavior.^{19–24} Overall, the electron–phonon, electron–electron, and electron–magnon scattering must be an important cause of resistivity in the FM metallic state of doped manganites.

The present investigations are structured as follows. In Sec. II, we first formulate an interaction potential, which

includes the long-range Coulomb, van der Waals (vdW) interaction, and the short-range repulsive interaction up to the second-neighbor ions within the Hafemeister and Flygare approach. This enables us to compute the Debye and Einstein temperatures of $\text{La}_{1-x}\text{Ag}_x\text{MnO}_3$ ($x = 0.05$ and 0.1). We use the Bloch–Gruneisen (BG) method to estimate the independent contributions of acoustic and optical phonons and both. Details of the numerical analysis and its results are discussed in Sec. III.

The main findings on $\text{La}_{1-x}\text{Ag}_x\text{MnO}_3$ ($x = 0.05$ and 0.1) manganites include:

(i) The computed Debye and Einstein temperatures from the interaction potential, which are consistent with the experimental results.

(ii) The optical phonon yields a relatively larger contribution to the resistivity compared to the contribution of acoustic phonon.

(iii) The classical electron–phonon model of resistivity, as the BG model partially describes the reported metallic resistivity behavior in the temperature range $T < T_{\text{MI}}$ for $\text{La}_{1-x}\text{Ag}_x\text{MnO}_3$ ($x = 0.05$ and 0.1).

(iv) The quadratic temperature dependence of $\rho_{\text{diff.}} [= \rho_{\text{exp.}} - \{\rho_0 + \rho_{e-\text{ph}}\}]$ is interpreted in terms of 3D electron–electron inelastic scattering.

(v) The $T^{4.5}$ dependence due to electron–magnon scattering is further required for a complete explanation.

(vi) The Mott–Ioffe–Regel criterion for metallic conductivity is valid, $k_Fl \sim 1$ and $\epsilon_F\tau \sim 1$.

The summary and our main conclusions are presented in Sec. IV.

II. METHOD OF COMPUTATION

Raman spectroscopy provides information about the electronic and lattice processes responsible for the physical behavior of the mixed valence manganites.²⁵ The ideal perovskite ABO_3 of cubic structure presents around 15 normal modes of vibration. The lowest frequency (external mode) corresponds to a vibration of the A ions against the rigid BO_6 octahedra. The intermediate frequency (bending mode) corresponds to a vibration where the B ion and two apical oxygens move against the other four oxygens of the octahedron. At the highest frequency (stretching mode), the B ion moves against the rigid oxygen octahedron.²⁶ We can thus model the phonon spectrum consisting of an acoustic branch of Debye type and a separated optical peak with characteristic Einstein temperature.

The understanding of the dynamical properties of materials requires the formulation of an effective interionic potential. To begin with, we made the following assumptions: The change in force constants is small; the short-range interactions are effective up to the second-neighbor ions; and the atoms are held together by harmonic elastic forces without any internal strains within the crystal.

We thus express the crystal energy for a particular lattice separation (r) as:

$$U(r) = U_C(r) + U_R(r) + U_V(r) . \quad (1)$$

The first term is the Coulomb energy and follows:

$$U_C(r) = -\sum_{ij} \frac{Z_i Z_j e^2}{r_{ij}} = -\frac{\alpha_m Z^2 e^2}{r} , \quad (2)$$

where α_m is the Madelung constant²⁷ and r_{ij} is the separation distance between i and j ions.

The short-range overlap repulsive energy is the second term in Eq. (1) and

$$\begin{aligned} U_R(r) = & nb\beta_{ij} \exp\left(\frac{r_i + r_j - r_{ij}}{\rho}\right) + n'b\beta_{ii} \exp\left(\frac{2r_i - kr_{ij}}{\rho}\right) \\ & + n'b\beta_{jj} \exp\left(\frac{2r_j - kr_{ij}}{\rho}\right) , \end{aligned} \quad (3)$$

follows Hafemeister and Flygare approach.²⁸ The ionic radii are r_i and r_j , k is the structure factor, and $n(n')$ is the number of the nearest (next nearest) ions, respectively. Furthermore, the notations b and ρ denote the hardness and range parameters, respectively.

The Pauling coefficients, β_{ij} , are defined in terms of valency [$Z_i(Z_j)$] and number of the outermost electrons [$n_i(n_j)$] in the anions (cations), respectively, as:

$$\beta_{ij} = 1 + (Z_i/n_i) + (Z_j/n_j) . \quad (4)$$

The last term in Eq. (1) is the vdW energy, denoted as:

$$U_V(r) = -\left(\sum_{ij} \frac{c_{ij}}{r_{ij}^6} + \sum_{ij} \frac{d_{ij}}{r_{ij}^8}\right) , \quad (5)$$

$$= -\left(\frac{C}{r^6} + \frac{D}{r^8}\right) , \quad (6)$$

due to dipole–dipole (d–d) and dipole–quadrupole (d–q) interactions. The abbreviations C and D represent the overall vdW coefficients, due to the interactions mentioned in Eq. (1), defined as²⁷:

$$C = c_{ij}S_6(r) + \frac{1}{2}(c_{ii} + c_{jj})S_6(0) , \quad (7)$$

and

$$D = d_{ij}S_8(r) + \frac{1}{2}(d_{ii} + d_{jj})S_8(0) , \quad (8)$$

where c_{ij} and d_{ij} are the vdW coefficients due to d–d and d–q interactions. We follow the variational method²⁹ to derive c_{ij} and d_{ij} as:

$$c_{ij} = \frac{3}{2} \frac{e\hbar}{\sqrt{m_e}} \alpha_i \alpha_j \left[(\alpha_i/N_i)^{1/2} + (\alpha_j/N_j)^{1/2} \right]^{-1} , \quad (9)$$

and

$$\begin{aligned} d_{ij} = & \frac{27}{8} \frac{\hbar^2}{m} \alpha_i \alpha_j \left[(\alpha_i/N_i)^{1/2} + (\alpha_j/N_j)^{1/2} \right]^2 \\ & \left[(\alpha_i/N_i) + \frac{20}{3} \left(\alpha_i \alpha_j / N_i N_j \right)^{1/2} + (\alpha_j/N_j) \right]^{-1} . \end{aligned} \quad (10)$$

Here, m_e is the electron mass, α_i is the electronic polarizability, and N_i denotes the effective number of electrons of the i th ion. The values of the overall vdW coefficients are obtained using Eqs. (7) and (8) and weighted in terms of appropriate lattice sums [$S_6(0)$, $S_6(r)$, $S_8(0)$, and $S_8(r)$].²⁷ The individual vdW coefficients c_{ij} and d_{ij} are obtained with certainty and accuracy as the excitation energies are ignored in Eqs. (9) and (10).³⁰

Herein, the above description we shall seek the interionic interaction in between a pair of ions such as Mn–O and La/Ag–O. It is clear from the above descriptions that the present effective interionic potential contains only two free parameters (b and ρ), which are determined from the equilibrium conditions^{31–34}:

$$\left(\frac{dU}{dr} \right)_{r=r_0} = 0 , \quad (11)$$

and bulk modulus

$$B_T = \frac{1}{9kr_0} \left(\frac{d^2U}{dr^2} \right)_{r=r_0} . \quad (12)$$

The model parameters obtained from Eqs. (11) and (12) have been used to compute the second order elastic constants (SOECs) (C_{11} , C_{12} , and C_{44}) as^{35,36}:

$$C_{11} = \frac{e^2}{4r_0^4} \left[-5.112 Z_m^2 + A_1 + \frac{(A_2 + B_2)}{2} \right] , \quad (13)$$

$$C_{12} = \frac{e^2}{r_0^4} \left[0.226 Z_m^2 - B_1 + \frac{(A_2 - 5B_2)}{2} \right] , \quad (14)$$

$$C_{44} = \frac{e^2}{4r_0^4} \left[2.556 Z_m^2 + B_1 + \frac{(A_2 + 3B_2)}{4} \right] , \quad (15)$$

where (A_1, B_1) and (A_2, B_2) are the short-range parameters for the nearest and the next nearest neighbors, respectively. These parameters are defined as³⁷:

$$A_1 = \frac{4r_0^3}{e^2} \left[\frac{d^2}{dr^2} V_{ij}(r) \right]_{r=r_0} , \quad (16)$$

$$A_2 = \frac{4(r_0\sqrt{2})^3}{e^2} \left[\frac{d^2}{dr^2} V_{ii}(r) + \frac{d^2}{dr^2} V_{jj}(r) \right]_{r=r_0\sqrt{2}} , \quad (17)$$

$$B_1 = \frac{4r_0^3}{e^2} \left[\frac{d}{dr} V_{ij}(r) \right]_{r=r_0} , \quad (18)$$

$$B_2 = \frac{4(r_0\sqrt{2})^2}{e^2} \left[\frac{d}{dr} V_{ii}(r) + \frac{d}{dr} V_{jj}(r) \right]_{r=r_0\sqrt{2}} , \quad (19)$$

where $V_{ij}(r)$ is the short-range potentials between the ions, which follow³⁸:

$$V_{ij}(r) = b\beta_{ij} \exp\left(\frac{r_i + r_j - r_{ij}}{\rho}\right) + c_{ij} r_{ij}^{-6} + d_{ij} r_{ij}^{-8} . \quad (20)$$

The elastic force constant κ is derived at the equilibrium interionic distance r_0 following²⁴:

$$\kappa = \frac{r_0}{2} [\pi^2 (C_{11} - C_{12})(C_{11} + C_{12} + 2C_{44})(C_{44})]^{\frac{1}{3}} . \quad (21)$$

Thus, we have estimated the elastic force constants in terms of the model Hamiltonian for a pair such as Mn–O and La/Ag–O and have the total elastic force constants of the Ag doped LaMnO_3 . This continuum model thus takes care of the clear physical binding in doped manganites. We stress that the simpler models based on this potential can describe those cohesive properties of such solids that depend on vdW interactions. However, the true potential must recognize the correct charge distribution and the relative orientations of the interacting atoms in manganites, which is a complicated task.

We shall now estimate the acoustic Debye branch characterized by the Debye temperature θ_D and an optical peak defined by the Einstein temperature θ_E . The Debye frequency is characterized as a cut-off frequency at the Brillouin zone boundary. It can be expressed in terms of the effective value of ionic mass and elastic force constant for crystal lattices with two different kinds of atoms such as Mn–O and La/Ag–O, which we deal with. The acoustic-mode and optical-mode frequencies are estimated in an ionic model using a value of effective ion charge $Ze = -2e$.³⁸

For the sake of simplicity, we have chosen an acoustic mass $M = (2M_+ + M_-)$ [Mn(O) which is symbolized by $M_+(M_-)$], $\kappa^* = 2\kappa$ for each directional oscillation mode to get the acoustic phonon frequency as^{22–24}:

$$\omega_D = \sqrt{\frac{2\kappa^*}{M}} . \quad (22)$$

In this regard, for a pairwise potential, the phonon is optic in origin and the frequency is determined by the reduced mass of the pair as $\mu^{-1} = M(A)^{-1} + M(B)^{-1}$, where A is the anion (La/Ag, Mn) and B is the cation (O).

$$\omega_{\text{LO}}^2 = \frac{\kappa + \alpha}{\mu} , \quad (23)$$

$$\omega_{\text{TO}}^2 = \frac{\kappa - \alpha}{\mu} , \quad (24)$$

where α is the force constant as

$$\alpha = \frac{8\pi}{3} \frac{(Ze)^2}{\Omega} . \quad (25)$$

ω_{LO} (ω_{TO}) symbolized for the longitudinal (transverse) optical phonon frequency and Ω for the volume of the unit cell.

It is known to us that in the metallic state, the electron–phonon, electron–electron, electron–magnon scattering, and polaronic effects are the major proponents of various conceptions in electrical transport. We shall begin with the description of the scattering of electron–phonon for the resistivity in the FM metallic state. To formulate a specific model, the temperature-dependent part of the metallic resistivity, following the Debye model, is^{19–24}:

$$\rho \approx \left(\frac{3}{\hbar e^2 v_F^2} \right) \frac{k_B T}{M v_s^2} \int_0^{2k_F} |F(q)|^2 \left[\frac{xq^3 dq}{[e^x - 1][1 - e^{-x}]} \right] , \quad (26)$$

with $x = \hbar\omega/k_B T$. In the above, $F(q)$ is the Fourier transform of the potential associated with one lattice site, v_F is the Fermi velocity, and v_s being the sound velocity. Eq. (26) in terms of acoustic phonon contribution determines the temperature dependence resistivity:

$$\rho_{\text{ac}}(T, \theta_D) = 4A_{\text{ac}} T(T/\theta_D)^4 \int_0^{\theta_D/T} x^5 (e^x - 1)^{-1} (1 - e^{-x})^{-1} dx , \quad (27)$$

where A_{ac} is a constant of proportionality defined as^{19–24}:

$$A_{\text{ac}} \cong \frac{3\pi^2 e^2 k_B}{k_F^2 v_s^2 L \hbar v_F^2 M} . \quad (28)$$

As the resistivity is additive, if the Matthiessen rule is obeyed, the resistivity is represented as a sum $\rho(T) = \rho_0 + \rho_{e-\text{ph}}(T)$, where ρ_0 is the residual resistivity that does not depend on temperature as electrons also scatter off impurities, defects, and disordered regions. However, in case of the Einstein type of phonon spectrum (an optical mode), $\rho_{\text{op}}(T)$ may be described as follows:

$$\rho_{\text{op}}(T, \theta_E) = A_{\text{op}} \theta_E^2 T^{-1} [e^{\theta_E/T} - 1]^{-1} [1 - e^{\theta_E/T}]^{-1} . \quad (29)$$

A_{op} is defined analogously to Eq. (28).

We have thus conveniently modeled the phonon resistivity in the FM metallic state by combining both terms arising from acoustic and optical phonons

$$\rho_{e-\text{ph}}(T) = \rho_{\text{ac}}(T, \theta_D) + \rho_{\text{op}}(T, \theta_E) . \quad (30)$$

The total resistivity follows:

$$\begin{aligned} \rho(T, \theta_D, \theta_E) &= \rho_0 + \rho_{\text{ac}}(T, \theta_D) + \rho_{\text{op}}(T, \theta_E) , \\ &= \rho_0 + 4A_{\text{ac}}(T/\theta_D)^4 T \times \int_0^{\theta_D/T} x^5 (e^x - 1)^{-1} (1 - e^{-x})^{-1} dx \\ &\quad + A_{\text{op}} \theta_E^2 T^{-1} [\exp(\theta_E/T) - 1]^{-1} [1 - \exp(-\theta_E/T)]^{-1} . \end{aligned} \quad (31)$$

The parent LaMnO_3 at high temperatures is an insulator with a cubic structure and becomes tetragonal due to distortions at low temperatures. Doping at a La site by Ca, Sr, Ba, Na, K, and so forth leads to a decrease not only in the structural phase transition temperature but also in the overall behavior of resistivity. However, for optimized doped $x \cong 0.3$, the material is still insulating (at about room temperature and higher) and the resistivity is much higher than the Mott limit. The substitution at the La site by divalent (monovalent) ions changes the valence of the Mn site as the outer Mn d -orbital shows two-fold degeneration and the result is Jahn–Teller (breathing type) distortion of the oxygen octahedra focused at each of the Mn occupied (unoccupied) sites. The energy required for the formation of a local lattice distortion is about 0.6 eV per site. Identifying a strong electron–phonon coupling and hence polaronic transport is essential in the doped materials. At high temperatures, the Jahn–Teller distortions are decorrelated, but do not disappear.³⁹

On the other hand, the double exchange mechanism shows that the oxygen ion is closed shell and supports hopping. In a true sense, an electron jumps onto a Mn

ion on the right simultaneously with an electron hopping onto the O ion from the Mn ion on the left. Henceforth, in the double hopping, both hopping electrons should have the same spin via the oxygen (O^{2-}) ions. Following Hund’s rule, the Mn^{3+} and Mn^{4+} ions should have the electron parallel spin moments for hopping. This mechanism connects the parallel alignment of Mn moments (ferromagnetism) with hopping of carriers (metallic conduction). Thus, an effective positive exchange coupling induced by the carriers was referred as double exchange.¹⁷

Actually, the lattice vibration of O ions essentially pushes the electrons toward vacant states in the Mn ion inducing a local distortion of the lattice. Such self-trapping of the charge carriers is substantially above the Curie temperature. However, below the Curie temperature, the self-trapping disappears because the bandwidth broadens and the electrons are much more mobile. It is inferred that at high temperature, the effective positive exchange coupling induced by the carriers does not solely

contribute to the resistivity and that a strong electron–phonon interaction arising from the Jahn–Teller splitting of the outer Mn d level is essentially required.⁴⁰

III. DISCUSSION AND ANALYSIS OF RESULTS

Any discussion of the mixed-valent oxides necessitates the knowledge of the structural aspects, and this is particularly true of the calculations reviewed here. Also applying the available informations on the developed theory inevitably entails certain complications and one has to find suitable data that vary from technique to technique. The phonon scattering mechanism herein is discussed within the Debye framework and the hopping of charge carriers is treated in an isotropic double exchange model. The validity of the Debye approximation lies in the fact that the temperature region of interest lies well below the Debye temperature. The phonon contribution in the continuum approximation is usually expressed in terms of relaxation time and is related to various scattering processes. Various relaxation rates are proportional to the imaginary part of the phonon self-energy.⁴¹

Special attention is paid in this approach to address the issue whether long range or short range interactions are at the origin of the transport properties of the monovalent Ag doped manganites. The effective interionic potential is thus constructed in an easily generalizable manner with realistic values of structural parameters, which actually control the resistivity behavior. The values of Debye and Einstein temperatures have been computed using the values of the two model parameters, namely, range (ρ), and hardness (b), for a pair such as La/Ag–O and Mn–O, which have been evaluated from the experimental values of equilibrium distance and bulk modulus.^{42–48}

The values of the overall vdW coefficients C and D involved in Eqs. (7) and (8) have been evaluated from the well-known Slater–Kirkwood variational methods,²⁹ which are listed in Table I. We use the A site ionic radii (La/Ag) as 1.13 Å. Within the continuum model, we notice that the hardness parameter (b_1 and b_2) increases and the range parameter (ρ_1 and ρ_2) decreases with the increased Ag doping concentration (x) in $\text{La}_{1-x}\text{Ag}_x\text{MnO}_3$. The model parameters and the SOECs are illustrated in Table II. The elastic force constant κ is derived at the equilibrium interionic distance r_0 following Eq. (21). The calculated values of κ are 5.695×10^5 and 6.042×10^5 gm s⁻² for $x = 0.05$ and 0.1 . Due to the lack of other theoretical calculations, the deduced value of model force constant could not be compared. Nevertheless, the evaluation of the elastic force constant gives a valuable guide to the behavior of vdW type forces in predicting the model phonon energies. Yet, the goal is not to determine the manner in which such interactions lead to the

description of phonon frequencies but to discuss the electrical resistivity behavior.

Finally, we evaluate the values of acoustic and optical phonon frequency (ω_D , ω_{LO} , and ω_{TO}) corresponding to Debye and Einstein temperatures. The computed values of ω_D , ω_{LO} , and ω_{TO} are presented in Table III. We must mention that these computed values of ω_D , ω_{LO} , and ω_{TO} for $\text{La}_{1-x}\text{Ag}_x\text{MnO}_3$ with ($x = 0.05$ and 0.1) could not be compared due to the lack of the experimental data. However, the computed values of Debye and Einstein temperatures for $\text{La}_{0.7}\text{Ba}_{0.3}\text{MnO}_3$ manganite following the model Hamiltonian approach yield consistent results.^{7,25,26,28,43,44,47,48}

It is true that the two-orbital model based on Wannier functions predicts the electronic states such as charge ordering in manganites. It is pointed out by Marzari et al. that the Wannier function approach of the electronic problem is useful for the description of electron dynamics following the semiclassical theory as well as the magnetic interactions in solids.⁴⁹ In the present investigation, we do not intend to discuss the electron dynamics as well the magnetic interactions, but focused on determining the acoustic (optical) phonon frequency to estimate the electron–phonon contribution of resistivity in the FM metallic phase.

The developed effective interionic interaction potential takes care of the interactions in between a pair such as Mn–O and La/Ag–O. The interactions, thus, are attractive Coulomb, and vdW as well as short-range overlap repulsive interaction following Hafemeister and Flygare

TABLE I. vdW coefficients of $\text{La}_{1-x}\text{Ag}_x\text{MnO}_3$ ($x = 0.05$ and 0.1) (c_{ij} in units of 10^{-60} erg cm⁶ and d_{ij} in units of 10^{-76} erg cm⁸).

x		c_{ii}	c_{ij}	c_{jj}	C	d_{ii}	d_{ij}	d_{jj}	D
$x = 0.05$	Mn–O	120.18	180.39	270.87	1543	131.53	193.35	284.10	1355
	La/Ag–O	16.93	63.53	270.87	679.09	22.76	80.75	284.10	619.0
	La/Ag–O	20.57	68.14	270.87	712.70	25.11	83.87	284.10	639.1

TABLE II. The model parameters (b , ρ) and the SOECs for $\text{La}_{1-x}\text{Ag}_x\text{MnO}_3$ ($x = 0.05$ and 0.1) samples.

x	Model parameters				SOECs		
	b_1 (La/Ag–O) (10^{-12} erg)	ρ_1 (La/Ag–O) (Å)	b_2 (Mn–O) (10^{-12} erg)	ρ_2 (Mn–O) (Å)	C_{11} (10^{12} Dyne cm ⁻²)	C_{12} (10^{12} Dyne cm ⁻²)	C_{44} (10^{12} Dyne cm ⁻²)
0.05	3.34	0.26	5.39	0.33	7.93	3.56	2.49
0.1	3.36	0.26	5.27	0.33	8.28	3.94	2.81

TABLE III. Parameters corresponding to the best fit to the experimental data of $\text{La}_{1-x}\text{Ag}_x\text{MnO}_3$ ($x = 0.05$ and 0.1) samples by using BG model.

x	T_{MI} (K)	ω_D (meV)	ω_{LO} (meV)	ω_{TO} (meV)	Parameters for resistivity		
					ρ_0 (Ω cm)	$A_{ac} \times 10^{-4}$ (Ω cm K ⁻¹)	$A_{op} \times 10^{-4}$ (Ω cm K ⁻¹)
0.05	272	47.86	68.37	74.44	0.0128	0.6	2.6
0.1	299	49.57	69.39	76.77	0.006	0.5	1.0

type potential. The advantage of using this potential is that it takes care of number of the nearest (next nearest) ions, the valency, and number of the outermost electrons in the anions (cations), respectively. Thus, it takes care of the structural parameters that yield an approximately correct description of the interactions between a pair such as Mn–O and La/Ag–O. Henceforth, we are able to estimate the acoustic (optical) phonon frequency consistent with the Raman measurements to estimate the electron–phonon contribution of resistivity.

We must refer to the work of Millis, who determines the elastic parameters using a mean field approximation with emphasis on Mn–O bond lengths and evaluated Mn–Mn and Mn–O force constants for the lattice distortions.³⁹ On the other hand, in the present model, we have considered both Mn–O and La/Ag–O bond lengths to obtain the Mn–O, La/Ag–O, and total force constants for strong electron–phonon interaction. The formulated effective interionic interaction potential includes the long-range Coulomb, vdW interaction, and the short-range repulsive interaction up to the second-neighbor ions within the Hafemeister and Flygare approach. The interionic interaction between a pair such as Mn–O and La/Ag–O enables us to find the total force constant with consistent Debye and Einstein temperatures.^{42–48}

To analyze the transport mechanism of the Ag substituted manganites with $x = 0.05$ and 0.1 in the intermediate-temperature FM region below T_p , we begin with the electron–phonon interaction to discuss the metallic behavior of $\rho(T)$. Figures 1 and 2 illustrate the results of temperature dependence of resistivity with the electron–phonon interaction from Eq. (31). The contributions of acoustic and optical phonon toward resistivity are clubbed and the resultant resistivity is exponential at low temperatures and nearly linear at high temperatures until transition temperature. In the following calculations, we have used residual resistivity¹¹ $\rho_0 \approx 0.021$ and $0.006 \Omega \text{ cm}$ for $x = 0.05$ and 0.1 . The coefficients A_{ac} (A_{op}) as functions of doping concentration are shown in Table III. It is noticed that the electron–phonon along with residual resistivity partially retraces the metallic resistivity behavior of $\text{La}_{1-x}\text{Ag}_x\text{MnO}_3$ with ($x = 0.05$ and 0.1) manganites and other temperature-dependent mechanisms such as electron–electron, and electron–magnon scattering should be invoked.

It is noticed from the plot that the estimated ρ is lower than the reported data from $T \cong 175$ K for $\text{La}_{1-x}\text{Ag}_x\text{MnO}_3$ with $x = 0.05$ and 0.1 to near the MI transition temperature (T_{MI}). The difference between the measured ρ and calculated ρ_{diff} [$= \rho_{\text{exp.}} - \{\rho_0 + \rho_{e-\text{ph}} (= \rho_{ac} + \rho_{op})\}$] is plotted in Fig. 3. A quadratic temperature dependence of $\rho_{\text{diff.}}$ is depicted at low temperature. The quadratic temperature contribution for resistivity is an indication of inelastic electron–electron

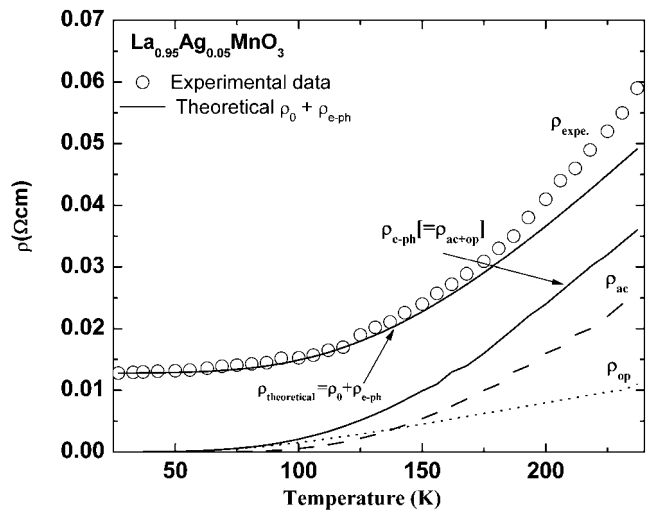


FIG. 1. Variation of $\rho_{e-\text{ph}}$ with temperature for $\text{La}_{0.95}\text{Ag}_{0.05}\text{MnO}_3$, the contribution of acoustic phonons ρ_{ac} as well as of optical phonons ρ_{op} to the resistivity. The solid line represents best fit to the equation: $\rho = \rho_0 + \rho_{e-\text{ph}} (= \rho_{ac} + \rho_{op})$. Circles represent the experimental data.¹¹

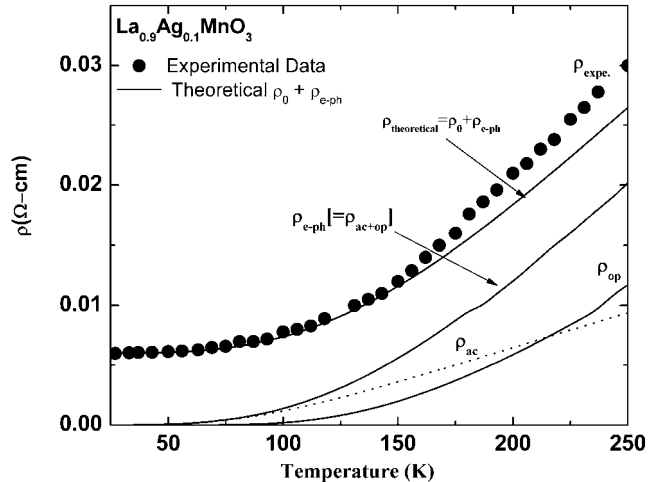


FIG. 2. Variation of $\rho_{e-\text{ph}}$ with temperature for $\text{La}_{0.9}\text{Ag}_{0.1}\text{MnO}_3$, the contribution of acoustic phonons ρ_{ac} as well as of optical phonons ρ_{op} to the resistivity. The solid line represents best fit to the equation: $\rho = \rho_0 + \rho_{e-\text{ph}} (= \rho_{ac} + \rho_{op})$. The circles represent the experimental data.¹¹

scattering. The electron–electron interaction and inelastic scattering of electrons in doped manganites are important in the explanation of electrical resistivity. The justifying of electron–electron interaction in doped manganites lies in a fact that these have a resistivity of $10\text{--}40 \text{ m}\Omega \text{ cm}$, which is higher than the Mott's maximum metallic resistivity ($\approx 10 \text{ m}\Omega \text{ cm}$).^{47,48}

The quadratic temperature dependence of $\rho_{\text{diff.}}$ is consistent with the earlier argument made.¹⁶ The additional term due to electron–electron contribution was required in understanding the resistivity behavior, as extensive attempts to fit the data with residual resistivity

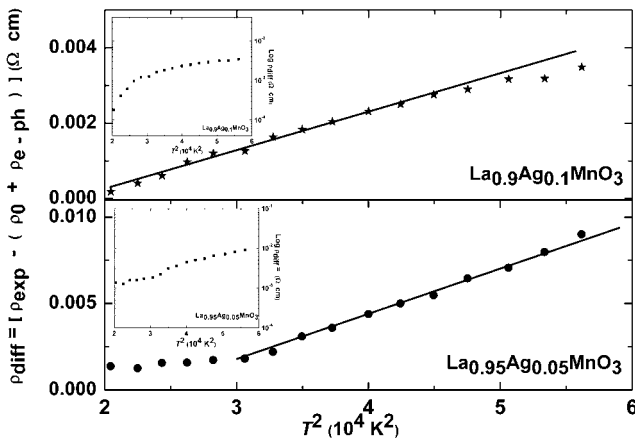


FIG. 3. Variation of $\rho_{\text{diff.}} [= \rho_{\text{exp.}} - \{\rho_0 + \rho_{e-\text{ph}} (= \rho_{\text{ac}} + \rho_{\text{op}})\}]$ with T^2 of $\text{La}_{1-x}\text{Ag}_x\text{MnO}_3$ ($x = 0.05$ and 0.1).

and phonon resistivity were unsuccessful. It is noteworthy to comment that in conventional metals, the electron–electron contribution to the resistivity can, at best, be seen only at very low temperatures, due to its small magnitude in comparison with the phonon contribution. The existence of quadratic temperature dependence of resistivity over a wide temperature interval permits one to believe that the electron–electron scattering is also significant in determining the resistivity in manganites.

We again refer to Fig. 3, where a substantial deviation from the T^2 -like behavior and a rapid rise in $\rho_{\text{diff.}}$ are observed in the intermediate temperature region ($175 < T < T_{\text{MI}}$) [please see the inset of Fig. 3, where $\log \rho_{\text{diff.}}$ is plotted as T^2 dependence]. We perform the similar set of exercises with the difference between the measured ρ and calculated $\rho_{\text{diff.}} [= \rho_{\text{exp.}} - \{\rho_0 + \rho_{e-\text{ph}} (= \rho_{\text{ac}} + \rho_{\text{op}})\}]$ beyond 175 K (plotted in Fig. 4). A $T^{4.5}$ temperature dependence of $\rho_{\text{diff.}}$ is depicted in higher temperature [please see the inset of Fig. 4 where $\log \rho_{\text{diff.}}$ is plotted as $T^{4.5}$ dependence]. The $T^{4.5}$ temperature contribution for resistivity is an indication of electron–magnon scattering. In the intermediate temperature region ($175 < T < T_{\text{MI}}$), the manganites appear to be normal metallic ferromagnet with the resistivity dominated by spin-wave scattering.

For hole doped manganites stressed that an additional $T^{4.5}$ contribution as a result of electron–magnon scattering process is essential.¹⁷ In the recent past, we have also noticed that the spin-wave scattering in the FM metallic phase is important in discussing the electrical resistivity behavior of $\text{La}_{0.67}\text{Ca}_{0.33}\text{MnO}_3$.¹⁹ We admit that in the higher temperature limit, the difference can be predicted linearly with $T^{4.5}$ in accord with the electron–magnon scattering in the double exchange process. The feature of $T^{4.5}$ temperature dependence of $\rho_{\text{diff.}}$ is consistent with the quantum theory of two-magnon scattering and is valid for half-metallic ferromagnets.¹⁷ Consequently, besides electron–phonon and electron–electron interactions, another possibility for the changes in carrier density

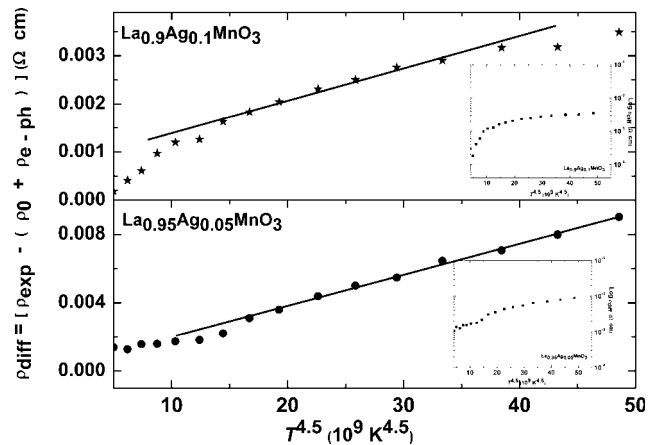


FIG. 4. Variation of $\rho_{\text{diff.}} [= \rho_{\text{exp.}} - \{\rho_0 + \rho_{e-\text{ph}} (= \rho_{\text{ac}} + \rho_{\text{op}})\}]$ with $T^{4.5}$ of $\text{La}_{1-x}\text{Ag}_x\text{MnO}_3$ ($x = 0.05$ and 0.1).

arose due to the presence of spin waves in the metallic system and is caused by spin-wave scattering.

We now address the metallic behavior of doped manganites. If the high-frequency phonon modes are indeed strongly coupling with charge carriers, the effective mass of the carriers should be substantially enhanced. The Fermi energy and the corresponding density of states are conveniently obtained from the thermo-electric power results⁵⁰ using $\epsilon_F = -\pi^2 k_B^2 T/[3|e|S_c^{\text{diff.}}(T)]$ and $N(\epsilon_F) = 3n_{3D}V/2\epsilon_F$ (where n_{3D} is the three-dimensional charge carrier density which is obtained following $n_{3D}d^3 = 1$ and V is the unit cell volume). The density of states in turn yields the electronic specific heat coefficient using $\gamma = (\pi k_B)^2 N(\epsilon_F)/3$ (see Table IV). It is noticed that the above values are consistent with the γ values in another hole doped divalent manganites^{51,52} and could not be compared due to the lack of experimental data on monovalent doped manganites. The effective mass of the carrier along the conducting Mn–O plane is deduced from electronic specific heat coefficient γ , using, $m^* = 3\hbar^2\pi\gamma d/k_B^2$.

The estimated electron parameters for $\text{La}_{1-x}\text{Ag}_x\text{MnO}_3$ with $x = 0.05$ and 0.1 are the Fermi wave vector k_F , the Fermi velocity v_F , and the plasma frequency ω_p and are given in Table IV. We stress that the effects induced by electron correlations and mass renormalizations by electron–electron interactions are crucial in magnetic systems such as doped manganites.^{53–57}

It is known that in conventional metals, electron–phonon scattering is mathematically identical to conventional impurity scattering and leads to a resistivity proportional to $(v_F^2 l)^{-1}$ where l is the mean free path. The mean free path in this approximation is usually related to the Fermi velocity and is estimated as follows $l = v_F \tau$. We follow the Drude relation, $\tau^{-1} = \rho_0 \omega_p^2 / 4\pi$, to obtain the scattering rate $R_s = \tau^{-1}$. The estimated values of R_s and l are given in Table IV. We must mention that the residual resistance obtained for nominally the same

TABLE IV. The estimated electron parameters for $\text{La}_{1-x}\text{Ag}_x\text{MnO}_3$ ($x = 0.05$ and 0.1) manganites.

x	ε_F (eV)	$N(\varepsilon_F) \times 10^{-19}$ (eV $^{-1}$ cm $^{-3}$)	γ (mJ mol $^{-1}$ K $^{-2}$)	M^*/m_e	$k_F \times 10^{-7}$ (cm $^{-1}$)	$v_F \times 10^{-7}$ (cm s $^{-1}$)	ω_p (eV)	$R_s \times 10^{-14}$ (s $^{-1}$)	l (Å)
0.05	0.48	9.83		8.614	4.724	3.764	9.19	0.993	3.371
0.1	0.83	5.73		5.023	2.754	3.764	1.57	1.301	1.652

compositions may vary significantly for different groups of compounds. It remains unclear whether ρ_0 only characterizes the sample's quality or if there is an intrinsic component in the residual resistivity.⁵⁸ For the Sr doped manganites, the resistivity data in the crystalline film yield ρ_0 as low as 10^{-5} Ω cm and are in the range of typical metallic conductors.⁵⁹ The deduced values of the Fermi energy (ε_F) for $\text{La}_{1-x}\text{Ag}_x\text{MnO}_3$ with $x = 0.05$ and 0.1 correspond to a narrow energy band. We notice that the Ag doped lanthanum manganites are good metals as the product $\varepsilon_F\tau \sim 1$.

The electron correlations in view of mass enhancement effect in narrow band materials are important in doped LaMnO_3 . We notice that enhanced electron mass $m^*/m_e > 1$ in $\text{La}_{1-x}\text{Ag}_x\text{MnO}_3$ (see Table IV) leads to the reduced plasma frequency, and hence the reduced zero temperature elastic scattering rate in comparison to conventional metals. It is perhaps worth noticing that the scattering rate at low temperatures is of the order of 10^{15} s $^{-1}$ in hole-doped manganites.¹⁷ Furthermore, the Mott–Ioffe–Regel criterion for metallic conductivity is valid, as the deduced mean free path is greater than the Mn–O bond length. The use of the BG expression in estimating the electron–phonon contributions is thus validated as the product $k_F l \sim 1$.

The monovalent Ag doped manganites thus illustrate a metallic behavior below metal–insulator transition temperature T_{MI} . The T_{MI} increases with the Ag doping concentration. With increased doping, the monovalent Ag doped manganites behave as good metals and are attributed to the fact that there are twice as many Mn $^{4+}$ ions as there are Ag ions and each of these Mn $^{4+}$ will contribute a hopping hole.

The effects of the grain-boundary-induced lattice disorder on the resistivity in $\text{Sm}_{0.55}\text{Sr}_{0.45}\text{MnO}_3$ at temperatures near the metal–insulator transition are carefully investigated.⁶⁰ The low temperature resistivity data ($T \leq 75$ K) of the SmSrMnO were successfully fitted using the relation $\rho = \rho_0 + \rho_2 T^2 + \rho_5 T^5$ with ρ_0 as the residual resistivity and ρ_2 and ρ_5 are the electron–electron and the electron–phonon scattering coefficients, respectively. It is further noticed that in this temperature range, the disorder does not affect the temperature dependence of ρ ; however, it causes an increase in the coefficients ρ_0 , ρ_2 , and ρ_5 by two orders of magnitude.

In contrast to electron–phonon scattering as the source of resistivity in FM metallic state, the angle-resolved photoemission spectroscopy data for the bilayer manganite $\text{La}_{1.2}\text{Sr}_{1.8}\text{Mn}_2\text{O}_7$ identify a coherent polaronic

metallic ground state below metal–insulator transition.⁶¹ The FM metallic state is a polaronic metal with a strong anisotropic character of the electronic excitations, strikingly similar to the pseudogap phases in heavily underdoped cuprate high temperature superconductors as Bi 2212. A strong mass enhancement and a small renormalization factor are found to account for the metallic properties.⁶² The temperature dependence of resistivity in the metallic state is intimately related to the polaronic metallic ground state and the insulator-to-metallic state can be attributed to the polaron coherence condensation process acting in concert with the double exchange mechanism. We may comment that the present theory finds an enhanced mass of holes as carrier ($m^*/m_e > 1$) for $\text{La}_{1-x}\text{Ag}_x\text{MnO}_3$ with $x = 0.05$ and 0.1 from the electronic specific heat coefficient to validate the Mott–Ioffe–Regel criterion. However, a detailed analysis is further required to understand the polaronic metallic state in the FM phase and the condensation process analogous to underdoped cuprate high temperature superconductors. We shall address this issue in near future.

Given that $\text{La}_{1-x}\text{Ag}_x\text{MnO}_3$ and related compounds are successfully used as magnetoresistive materials, a careful and complete study of their magnetic, transport, and structural properties is essentially required for technological applications. These magnetic materials witness a transition from a high temperature FM insulating phase to either a lower temperature FM metallic phase or AF insulating phase. The transition seen is associated with a large drop in electrical resistivity under the application of a magnetic field and leads to a large CMR. A careful study reveals that the Zener double exchange model, a strong electron–phonon interaction and polaron transport, is successful in explaining the electrical resistivity in the insulating and metallic phases of these manganites.⁶³

A minimum in the resistivity under the application of magnetic field is also important in manganites. The low temperature resistivity minimum is seen in noble-metal alloys with magnetic impurity and is explained in terms of Kondo effect (logarithmic dependence of resistivity on temperature). It arises from the exchange interaction between itinerant conduction electrons and localized spin impurities along with electron–electron interaction predicted the resistivity minima in $\text{La}_{2/3}\text{Ca}_{1/3}\text{MnO}_3$. The upturn of resistivity below minimum resistivity could be due to factors like the Kondo effect or the electron–electron interaction. The expression used for a successful fit includes resistivity due to the domain boundaries, electron–electron interaction, spin-disorder scattering,

Kondo term, and electron–phonon scattering is: $\rho(T) = 1/[\rho_0 + \rho_e T^{1/2}] + \rho_{\text{spin}} \ln T + \rho_{e-\text{ph}} T^5$.⁶⁴

The magnetoresistivity in manganites at low temperatures needs a careful understanding of electrical resistivity. Schiffer and researchers argued that the resistivity in doped manganites follows using the relation $\rho = \rho_0 + \rho_{2.5} T^{2.5}$.⁶⁵ Here, ρ_0 is the residual and other temperature-independent scattering mechanisms. The term $\rho_{2.5} T^{2.5}$ is an empirical fit to the data, which represents a combination of electron–electron, electron–phonon, and electron–magnon scattering. Figures 5 and 6 illustrate the results of temperature dependence of resistivity in $\text{La}_{1-x}\text{Ag}_x\text{MnO}_3$ ($x = 0.05$ and 0.1) manganites using $\rho = \rho_0 + \rho_{2.5} T^{2.5}$. The best-fit parameters are $\rho_0 = 0.0128$ (0.006) $\Omega \text{ cm}$ and

$\rho_{2.5} = 4.59$ (2.5) $\times 10^{-8} \Omega \text{ cm/K}^{2.5}$ for $\text{La}_{0.95}\text{Ag}_{0.05}\text{MnO}_3$ ($\text{La}_{0.90}\text{Ag}_{0.10}\text{MnO}_3$).

We note that empirical $T^{2.5}$ dependence, although retraces the curve, but, the data are not fitted adequately. Deduced values of $\rho_{2.5}$ are consistent with earlier findings on $\text{La}_{0.85}\text{Te}_{0.15}\text{Mn}_{1-x}\text{Cu}_x\text{O}_3$ ($0 \leq x \leq 0.20$) in the intermediate-temperature FM metallic region below the Curie temperature.⁶⁶ It is further argued that rather taking independent temperature dependencies of various scattering mechanisms as electron–electron scattering process ($\rho_{ee} T^2$), electron–magnon scattering process in the FM metallic phase ($\rho_{\text{spin wave}} T^{4.5}$) as $\rho = \rho_0 + \rho_{e-e} T^{2.5} + \rho_{\text{spin wave}} T^{4.5}$, it is better to represent resistivity in terms of a combination of electron–electron, electron–phonon, and electron–magnon scattering with $\rho_{2.5} T^{2.5}$ form.⁶⁷

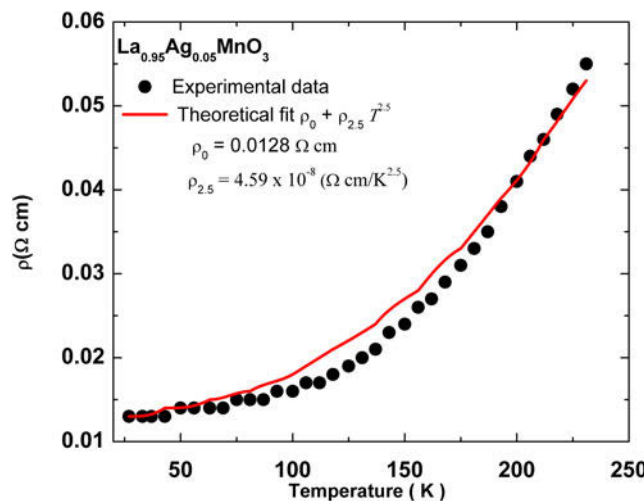


FIG. 5. Variation of resistivity (ρ) with temperature for $\text{La}_{0.95}\text{Ag}_{0.05}\text{MnO}_3$. The solid line represents best fit to the equation: $\rho = \rho_0 + \rho_{2.5} T^{2.5}$. The circles represent the experimental data.¹¹

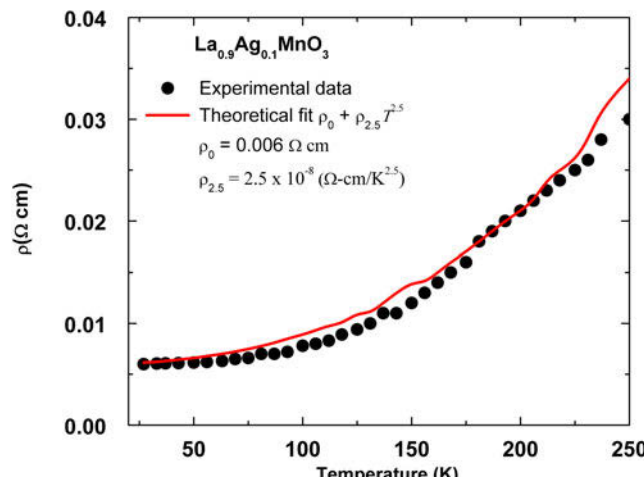


FIG. 6. Variation of resistivity (ρ) with temperature for $\text{La}_{0.9}\text{Ag}_{0.1}\text{MnO}_3$. The solid line represents best fit to the equation: $\rho = \rho_0 + \rho_{2.5} T^{2.5}$. The circles represent the experimental data.¹¹

IV. CONCLUSION

Either double exchange mechanisms or small polarons have primarily described the physics of manganites. The behavior of electrical resistivity in doped manganites explicitly the monovalent doped ion needs more clarification. The reported behavior of electrical resistivity in Ag doped manganites in the FM metallic phase is analyzed in the framework of the additional model of electron–phonon interaction using the model phonon spectrum consisting of two parts: An acoustic branch of Debye type and optical mode with characteristic Einstein temperature. Deduced values of Debye and Einstein temperatures from the pairwise potential with the long-range Coulomb, vdW interaction, and the short-range repulsive interaction up to the second-neighbor ions within the Hafemeister and Flygare approach are consistent with Raman spectroscopy measurements. For the sake of simplicity, a single (longitudinal and transverse) optical phonon mode has been considered, with a flat dispersion relation.

The high-energy optical phonon yields a large contribution to the resistivity and is attributed to a significant optical phonon hardening effect on carrier transport. From such a fitting, signatures of different types of interaction terms as electron–phonon, electron–electron, and electron–magnon are found to govern the transport mechanism in the low-temperature FM metallic phase ($T < T_{MI}$). The temperature-dependent resistivity data in this region, where the local FM order is almost complete, have been successfully fitted with $\rho = \rho_0 + \rho_{e-\text{ph}} + \rho_{e-e}(T^2) + \rho_{e-\text{mag}}(T^{4.5})$. We may comment that apart from the resistivity due to domain, grain-boundary and the electron–phonon scattering, the electron–electron and electron–magnon scattering are essential for a complete description of the metallic behavior of $\text{La}_{1-x}\text{Ag}_x\text{MnO}_3$ with $x = 0.05$ and 0.1 manganites.

We have also attempted to fit the resistivity behavior using the empirical relation ($= \rho_0 + \rho_{2.5} T^{2.5}$). The second-term $\rho_{2.5} T^{2.5}$ represents a combination of

electron-electron, electron-phonon, and electron-magnon scattering. It is noted that empirical $T^{2.5}$ dependence, although retraces the curve, but the data are not fitted adequately. The mean free path is larger than the Mn–O bond length and the product of $k_F l \sim 1$ and $\varepsilon_{\text{FT}} \sim 1$ favors metallic conduction. Hence, it is appropriate to use the BG expression in estimating the electron-phonon contributions at $T < T_{\text{MI}}$, and this is associated with the dynamic Jahn-Teller distortion, arising from the local lattice distortion due to the strong electron-phonon coupling. We finally conclude that below the Curie temperature, i.e., in the FM metallic phase two mechanisms are responsible for the resistivity: A temperature-independent scattering of the electrons (due to domain and grain boundaries, defects, etc.) and other temperature-dependent mechanisms (electron-electron, electron-phonon, and electron-magnon scattering).

ACKNOWLEDGMENT

Financial assistance from MPCST, Bhopal, India is gratefully acknowledged.

REFERENCES

1. M.B. Salamon and M. Jaime: The physics of manganites: Structure and transport. *Rev. Mod. Phys.* **73**, 583 (2001).
2. C. Zener: Interaction between the d shells in the transition metals. II. Ferromagnetic compounds of manganese with perovskite structure. *Phys. Rev.* **82**, 403 (1951).
3. P.W. Anderson and H. Hasegawa: Considerations on double exchange. *Phys. Rev.* **100**, 675 (1955).
4. A.J. Millis, P.B. Littlewood, and B.I. Shraiman: Double exchange alone does not explain the resistivity of $\text{La}_{1-x}\text{Sr}_x\text{MnO}_3$. *Phys. Rev. Lett.* **74**, 5144 (1995).
5. S. Roy, Y.Q. Guo, S. Venkatesh, and N. Ali: Interplay of structure and transport properties of sodium-doped lanthanum manganite. *J. Phys.: Condens. Matter* **13**, 9547 (2001).
6. R.D. Shannon: Revised effective ionic radii and systematic studies of interatomic distances in halides and chalcogenides. *Acta Crystallogr., Sect. A: Found. Crystallogr.* **32**, 751 (1976).
7. M.V. Abrashev, A.P. Litvinchuk, M.N. Iliev, R.L. Meng, V.N. Popov, V.G. Ivanov, R.A. Chakalov, and C. Thomsen: Comparative study of optical phonons in the rhombohedrally distorted perovskites LaAlO_3 and LaMnO_3 . *Phys. Rev. B* **59**, 4146 (1999).
8. A.J. Millis, B.I. Shraiman, and R. Mueller: Dynamic Jahn-Teller effect and colossal magnetoresistance in $\text{La}_{1-x}\text{Sr}_x\text{MnO}_3$. *Phys. Rev. Lett.* **77**, 175 (1996).
9. C. Sen, G. Alvarez, and E. Dagotto: Competing ferromagnetic and charge-ordered states in models for manganites: The origin of the colossal magnetoresistance effect. *Phys. Rev. Lett.* **98**, 127202 (2007).
10. R. Yu, S. Dong, C. Sen, G. Alvarez, and E. Dagotto: Short-range spin and charge correlations and local density of states in the colossal magnetoresistance regime of the single-orbital model for manganites. *Phys. Rev. B* **77**, 214434 (2008).
11. S.L. Ye, W.H. Song, J.M. Dai, K.Y. Wang, S.G. Wang, C.L. Zhang, J.J. Du, Y.P. Sun, and J. Fang: Effect of Ag substitution on the transport property and magnetoresistance of LaMnO_3 . *J. Magn. Magn. Mater.* **248**, 26 (2002).
12. S. Kumar and P. Majumdar: Singular effect of disorder on electronic transport in strongly coupled electron-phonon systems. *Phys. Rev. Lett.* **94**, 136601 (2005).
13. S. Kumar and P. Majumdar: Insulator-metal phase diagram of the optimally doped manganites from the disordered Holstein-double exchange model. *Phys. Rev. Lett.* **96**, 016602 (2006).
14. A.S. Alexandrov, G.-m. Zhao, H. Keller, B. Lorenz, Y.S. Wang, and C.W. Chu: Evidence for polaronic Fermi liquid in manganites. *Phys. Rev. B* **64**, 140404 (2001).
15. G.-m. Zhao, V. Smolyaninova, W. Prellier, and H. Keller: Electrical transport in the ferromagnetic state of manganites: Small-polaron metallic conduction at low temperatures. *Phys. Rev. Lett.* **84**, 6086 (2000).
16. M. Jaime, P. Lin, M.B. Salamon, and P.D. Han: Low-temperature electrical transport and double exchange in $\text{La}_{0.67}(\text{Pb}, \text{Ca})_{0.33}\text{MnO}_3$. *Phys. Rev. B* **58**, R5901 (1998).
17. K. Kubo and N. Ohata: A quantum theory of double exchange. *J. Phys. Soc. Jpn.* **33**, 21 (1972).
18. A.S. Alexandrov and A.M. Bratkovsky: Carrier density collapse and colossal magnetoresistance in doped manganites. *Phys. Rev. Lett.* **82**, 141 (1999).
19. D. Varshney and N. Kaurav: Electrical resistivity in the ferromagnetic metallic state of $\text{La}-\text{Ca}-\text{MnO}_3$: Role of electron-phonon interaction. *Eur. Phys. J. B* **40**, 129 (2004).
20. D. Varshney and N. Kaurav: Interpretation of temperature-dependent resistivity of $\text{La}-\text{Pb}-\text{MnO}_3$: Role of electron-phonon interaction. *J. Low Temp. Phys.* **141**, 165 (2005).
21. D. Varshney, I. Mansuri, and N. Kaurav: Effect of electron/hole doping on the transport properties of lanthanum manganites LaMnO_3 . *J. Phys.: Condens. Matter* **19**, 24 (2007).
22. D. Varshney, M.W. Shaikh, and I. Mansuri: Interpretation of temperature-dependent resistivity of $\text{La}_{0.7}\text{Ba}_{0.3}\text{MnO}_3$ manganites. *J. Alloys Compd.* **486**, 726 (2009).
23. D. Varshney, D. Choudhary, and M.W. Shaikh: Interpretation of metallic and semiconducting temperature dependent resistivity of $\text{La}_{1-x}\text{Na}_x\text{MnO}_3$ ($x = 0.07, 0.13$) manganites. *Comput. Mater. Sci.* **47**, 839 (2010).
24. D. Varshney, D. Choudhary, and M.W. Shaikh: Electrical resistivity behavior of sodium substituted manganites: Electron-phonon, electron-electron and electron-magnon interactions. *Eur. Phys. J. B* **76**, 327 (2010).
25. M.N. Iliev, M.V. Abrashev, H-G. Lee, V.N. Popov, Y.Y. Sun, C. Thomsen, R.L. Meng, and C.W. Chu: Raman spectroscopy of orthorhombic perovskite like YMnO_3 and LaMnO_3 . *Phys. Rev. B* **57**, 2872 (1998).
26. E. Granado, N.O. Moreno, A. García, J.A. Sanjurjo, C. Rettori, I. Torriani, S.B. Oseroff, J.J. Neumeier, K.J. McClellan, S-W. Cheong, and Y. Tokura: Phonon Raman scattering in $\text{R}_{1-x}\text{A}_x\text{MnO}_{3+\delta}$ ($\text{R} = \text{La}, \text{Pr}; \text{A} = \text{Ca}, \text{Sr}$). *Phys. Rev. B* **58**, 11435 (1988).
27. M.P. Tosi: Cohesion of ionic solids in the Born model. *Solid State Phys.* **16**, 1 (1964).
28. D.W. Hafemeister and W.H. Flygare: Outer-shell overlap integral as a function of distance for halogen-halogen, halogen-alkali, and alkali-alkali ions in the alkali halide lattices. *J. Chem. Phys.* **43**, 795 (1965).
29. J.C. Slater and J.G. Kirkwood: The van der Waals forces in gases. *Phys. Rev.* **37**, 682 (1931).
30. D. Varshney, N. Kaurav, R. Kinge, and R.K. Singh: B1–B2 structural phase transition and elastic properties of UX ($\text{X} = \text{S}, \text{Se}$, and Te) compounds at high pressure. *J. Phys.: Condens. Matter* **19**, 236204 (2007).
31. D. Varshney, G. Joshi, M. Varshney, and S. Shriya: Pressure dependent elastic and structural ($B3-B1$) properties of Ga based monopnictides. *J. Alloys Compd.* **495**, 23 (2009).

32. D. Varshney, V. Rathore, R. Kinge, and R.K. Singh: High-pressure induced structural phase transition in alkaline earth CaX ($X = \text{S}, \text{Se}$ and Te) semiconductors: NaCl -type (B1) to CsCl -type (B2). *J. Alloys Compd.* **484**, 239 (2009).
33. D. Varshney, G. Dagaonkar, and M. Varshney: Pressure and doping dependent elastic and thermodynamical properties of $\text{Ga}_{1-x}\text{In}_x\text{P}$ mixed valent compounds. *Mater. Res. Bull.* **45**, 916 (2010).
34. D. Varshney, G. Joshi, M. Varshney, and S. Shriya: Pressure induced structural phase transition and elastic properties in BSb , AlSb , GaSb and InSb compounds. *Phys. B* **405**, 1663 (2010).
35. D. Varshney, G. Joshi, M. Varshney, and S. Shriya: Pressure induced mechanical properties of boron based pnictides. *Solid State Sci.* **12**, 864 (2010).
36. D. Varshney, S. Shriya, and M. Varshney: Study of pressure induced structural phase transition and elastic properties of lanthanum pnictides. *Eur. Phys. J. B* **85**, 241 (2012).
37. D. Varshney: Mechanical, and elastic properties of europium mono-oxides and mono-chalcogenides ($\text{EuX}; X = \text{O}, \text{S}, \text{Se}, \text{Te}$). *Europium: Synthesis, Characteristics and Potential Applications*, M.S. Attia, ed.; Nova Science Publication, New York, (2013).
38. D. Varshney and S. Shriya: Elastic, mechanical and thermodynamic properties at high pressures and temperatures of transition metal monocarbides. *Int. J. Refract. Met. Hard Mater.* **41**, 375 (2013).
39. A.J. Millis: Cooperative Jahn-Teller effect and electron-phonon coupling in $\text{La}_{1-x}\text{A}_x\text{MnO}_3$. *Phys. Rev. B* **53**, 8434 (1996).
40. C. Ederer, C. Lin, and A.J. Millis: Structural distortions and model Hamiltonian parameters: From LSDA to a tight-binding description of LaMnO_3 . *Phys. Rev. B* **76**, 155105 (2007).
41. D. Varshney: Effect of impurity scatterers on phonon, electron and magnon thermal transport in electron doped cuprate superconductors. *Supercond. Sci. Technol.* **19**, 433 (2006).
42. D. Varshney and I. Mansuri: Influence of Ce doping on structural and transport properties of $\text{Ca}_{1-x}\text{Ce}_x\text{MnO}_3$ ($x = 0.2$) manganite. *J. Low Temp. Phys.* **162**, 52 (2011).
43. I. Mansuri, D. Varshney, N. Kaurav, C.L. Lu, and Y.K. Kuo: Effects of A-site disorder on magnetic, electrical and thermal properties of $\text{La}_{0.5-x}\text{Ln}_x\text{Ca}_{0.5-y}\text{Sr}_y\text{MnO}_3$ manganites. *J. Magn. Magn. Mater.* **323**, 316 (2011).
44. D. Varshney, N. Dodiya, and M.W. Shaikh: Structural properties and electrical resistivity of Na-substituted lanthanum manganites: $\text{La}_{1-x}\text{Na}_x\text{MnO}_{3+y}$ ($x = 0.1, 0.125$ and 0.15). *J. Alloys Compd.* **509**, 7447 (2011).
45. D. Varshney and N. Dodiya: Interpretation of metallic and semiconducting temperature dependent resistivity of $\text{La}_{0.91}\text{Rb}_{0.06}\text{Mn}_{0.94}\text{O}_3$ manganites. *Solid State Sci.* **13**, 1623 (2011).
46. D. Varshney and N. Dodiya: Electrical resistivity of the hole doped $\text{La}_{0.8}\text{Sr}_{0.2}\text{MnO}_3$ manganites: Role of electron-electron/phonon/magnon interactions. *Mater. Chem. Phys.* **129**, 896 (2011).
47. I. Mansuri and D. Varshney: Structure and electrical resistivity of $\text{La}_{1-x}\text{Ba}_x\text{MnO}_3$ ($0.25 \leq x \leq 0.35$) perovskites. *J. Alloys Compd.* **513**, 256 (2012).
48. M.W. Shaikh and D. Varshney: Structural properties and electrical resistivity behavior of $\text{La}_{1-x}\text{K}_x\text{MnO}_3$ ($x = 0.1, 0.125$ and 0.15) manganites. *Mater. Chem. Phys.* **134**, 886 (2012).
49. N. Marzari and D. Vanderbilt: Maximally localized generalized Wannier functions for composite energy bands. *Phys. Rev. B* **56**, 12847 (1997).
50. I.K. Kamilov, A.G. Gamzatov, A.M. Aliev, A.B. Batdalov, Sh.B. Abdulgaidov, O.V. Mel'nikov, O.Yu. Gorbenko, and A.R. Kaul: Kinetic effects in manganites $\text{La}_{1-x}\text{Ag}_y\text{MnO}_3$ ($y \leq x$). *J. Exp. Theor. Phys.* **105**, 774 (2007).
51. L. Ghivelder, I.A. Castillo, N. McN Alford, G.J. Tomka, P.C. Riedi, J. MacManus-Driscoll, A.K.M. Akther Hossain, and L.F. Cohen: Specific heat of $\text{La}_{1-x}\text{Ca}_x\text{MnO}_{3-\delta}$. *J. Magn. Magn. Mater.* **189**, 274 (1998).
52. D. Varshney, I. Mansuri, N. Kaurav, W.Q. Lung, and Y.K. Kuo: Influence of Ce doping on electrical and thermal properties of $\text{La}_{0.7-x}\text{Ce}_x\text{Ca}_{0.3}\text{MnO}_3$ ($0.0 \leq x \leq 0.7$) manganites. *J. Magn. Magn. Mater.* **324**, 3276 (2012).
53. N. Dodiya and D. Varshney: Structural properties and Raman spectroscopy of rhombohedral $\text{La}_{1-x}\text{Na}_x\text{MnO}_3$ ($0.075 \leq x \leq 0.15$). *J. Mol. Struct.* **1031**, 104 (2013).
54. D. Varshney, D. Choudhary, and E. Khan: Electrical transport in the ferromagnetic and paramagnetic state of potassium substituted manganites $\text{La}_{1-x}\text{K}_x\text{MnO}_3$ ($x = 0.05, 0.1$ and 0.15). *J. Mater. Sci.* **48**, 5904 (2013).
55. D. Varshney and N. Dodiya: Electrical resistivity of alkali metal doped manganites $\text{La}_x\text{A}_y\text{Mn}_w\text{O}_3$ ($\text{A} = \text{Na}, \text{K}, \text{Rb}$): Role of electron-phonon, electron-electron and electron-magnon interactions. *Curr. Appl. Phys.* **13**, 1188 (2013).
56. D. Varshney, I. Mansuri, M.W. Shaikh, and Y.K. Kuo: Effect of Fe and Co doping on electrical and thermal properties of $\text{La}_{0.5}\text{Ce}_{0.5}\text{Mn}_{1-x}(\text{Fe},\text{Co})_x\text{O}_3$ manganites. *MRS Bulletin* **48**, 4606 (2013).
57. D. Varshney and N. Dodiya: Structural and magnetotransport studies of magnetic ion doping for monovalent-doped LaMnO_3 manganites. *J. Mater. Res.* **29**, 1183 (2014).
58. M. Quijada, J. Cerne, J.R. Simpson, H.D. Drew, K.H. Ahn, A.J. Millis, R. Shreekala, R. Ramesh, M. Rajeswari, and T. Venkatesan: Optical conductivity of manganites: Crossover from Jahn-Teller small polaron to coherent transport in the ferromagnetic state. *Phys. Rev. B* **58**, 16093 (1998).
59. A. Urushibara, Y. Moritomo, T. Arima, A. Asamitsu, G. Kido, and Y. Tokura: Insulator-metal transition and giant magnetoresistance in $\text{La}_{1-x}\text{Sr}_x\text{MnO}_3$. *Phys. Rev. B* **51**, 14103 (1995).
60. M. Egilmez, K.H. Chow, J. Jung, I. Fan, A.I. Mansour, and Z. Salman: Metal-insulator transition, specific heat, and grain-boundary-induced disorder in $\text{Sm}_{0.55}\text{Sr}_{0.45}\text{MnO}_3$. *Appl. Phys. Lett.* **92**, 132505 (2008).
61. N. Mannella, W.L. Yang, K. Tanaka, X.J. Zhou, H. Zheng, J.F. Mitchell, J. Zaanen, T.P. Devereaux, N. Nagaosa, Z. Hussain, and Z.X. Shen: Polaron coherence condensation as the mechanism for colossal magnetoresistance in layered manganites. *Phys. Rev. B* **76**, 233102 (2007).
62. N. Mannella, W.L. Yang, X.J. Zhou, H. Zheng, J.F. Mitchell, J. Zaanen, T.P. Devereaux, N. Nagaosa, Z. Hussain, and Z.X. Shen: Nodal quasiparticle in pseudogapped colossal magnetoresistive manganites. *Nature* **438**, 474 (2005).
63. P. Graziosi, A. Gambardella, M. Prezioso, A. Riminiucci, I. Bergenti, N. Homonay, G. Schmidt, D. Pullini, and D. Busquets-Mataix: Polaron framework to account for transport properties in metallic epitaxial manganite films. *Phys. Rev. B* **89**, 214411 (2014).
64. Z. Chen, Y. Xu, Y. Su, S. Cao, and J. Zhang: Resistivity minimum behavior and weak magnetic disorder characteristics in $\text{La}_{2/3}\text{Ca}_{1/3}\text{MnO}_3$ manganites. *J. Supercond. Novel Magn.* **22**, 465 (2009).
65. P. Schiffer, A.P. Ramirez, W. Bao, and S-W. Cheong: Low temperature magnetoresistance and the magnetic phase diagram of $\text{La}_{1-x}\text{Ca}_x\text{MnO}_3$. *Phys. Rev. Lett.* **75**, 3335 (1995).
66. R. Ang, Y.P. Sun, J. Yang, X.B. Zhu, and W.H. Song: Transport mechanism and magnetothermoelectric power of electron-doped manganites $\text{La}_{0.85}\text{Te}_{0.15}\text{Mn}_{1-x}\text{Cu}_x\text{O}_3$ ($0 \leq x \leq 0.2$). *J. Appl. Phys.* **100**, 073706 (2006).
67. J.M. De Teresa, M.R. Ibarra, J. Blasco, J. García, C. Marquina, and P.A. Algarabel, Z. Arnold and K. Kamenev, C. Ritter, and R. von Helmolt: Spontaneous behavior and magnetic field and pressure effects on $\text{La}_{2/3}\text{Ca}_{1/3}\text{MnO}_3$ perovskite. *Phys. Rev. B* **54**, 1187 (1996).